Supporting Information

Pratt et al. 10.1073/pnas.1308531111

SI Materials and Methods

Plasmid Construction and Protein Preparation. BL21 cells (Novagen) instead of $SOD^{-/-}$ *Escherichia coli* were used for protein expression, 100 mM each $CuSO_4$ and $ZnSO_4$ were substituted for $MgCl_2$ during osmotic shock, and $AmSO_4$-precipitated protein was removed with an additional centrifugation step before sample loading onto a 5-mL Phenyl-Sepharose FF (high substitution) column (GE Healthcare). Protein was dialyzed against 10 mM Tris (pH 7.5), separated on a 5-mL Q HP column (GE Healthcare) instead of a POROS HS ion exchange column, and eluted using a 0- to 250-mM NaCl gradient. Before metal reconstitution, protein samples were subjected to a final purification step in 20 mM Tris (pH 8) and 0.5 M NaCl on a Sephacryl S100 column (GE Healthcare). WT SOD and its ALS variants coexpressed with CCS were prepared as described (1), with minor changes. PMSF and EDTA were omitted from the lysis buffer, EDTA-free Complete (Roche) tablets were used, and the second ammonium sulfate step was omitted. For both methods, 1 mM β-mercaptoethanol (BME) was included in all purification steps, and final protein samples were buffer-exchanged into PBS (pH 7.4) before flash cooling and storage at 10 mg/mL at −80 °C. Apo-SOD samples were prepared by dialysis as described (2).

Protein Analysis, Metal Analysis, and Aggregation Conditions. For initial experiments, 50 mM citric acid–Na_2HPO_4 (pH 3.5), 150 mM NaCl, and 1 mM EDTA substituted for PBS/EDTA, and reactions proceeded for 0.5–48 h. For experiments <2 d, 1 mM BME was added to the reaction, whereas for extended time courses, pH-neutralized 0.25 mM Tris-(2-carboxyethyl)phosphine was used. Different A_{280} extinction coefficient values have been used in the literature to calculate SOD protein concentration [0.32 (3), 0.3375 (4), or 0.3 $mL{\cdot}mg^{-1}{\cdot}cm^{-1}$ (5)] based on the absorbance of the bound copper that contributes at 265 nm. The mutants prepared in this study displayed a wide range of metallation, with none at 100% copper incorporation, and therefore, we determined protein concentration using a consistent value of 0.365 $mL{\cdot}mg^{-1}{\cdot}cm^{-1}$ based on the protein sequence.

Protein samples in PBS with 1 mM BME were diluted to 1.3 mL in 2% (vol/vol) nitric acid, incubated at 37 °C with shaking at 250 rpm for 1.5 h, and then centrifuged. Samples and matching buffers were analyzed for copper and zinc content on an octopole-based 7500ce Inductively Coupled Plasma Mass Spectrometer using a MicroMist Nebulizer (Agilent Technologies).

DLS. Ten measurements were recorded for each sample, and the raw data were analyzed by using the Dynamics 7.1.7 software package with a regularization model to derive the radii of hydration.

SAXS and Graphical Analyses. The X-ray wavelength (λ) was 1.03 Å with a sample-to-detector distance of 1.5 m, and the beam size at the sample was 5.0 × 0.5 mm (6). The scattering vector q ($q = 4\pi \sin\theta/\lambda$, where 2θ is the scattering angle) range was 0.01–0.32 $Å^{-1}$. X-ray exposures between 0.5 and 5 s were taken for each sample and matching buffer blank, and the scattering of the buffer was subtracted from that of the protein. Datasets were merged with PRIMUS (7). Comparable profiles were observed for SOD samples from 2.5 to 10 mg/mL under physiological conditions, and samples of 2 mg/mL were used for aggregation experiments. The $P(r)$ function, R_g (real-space approximation), and maximum distance D_{max} were calculated with GNOM (8). Ten independent ab initio modeling jobs for WT SOD were performed using DAMMIN (9) (P2 symmetry) and averaged using DAMAVER (10). The best and worst models had χ^2 values of 1.65 and 1.73, respectively, and the average normalized spatial discrepancy was 0.65 ± 0.06. For aggregated G93A data, modeling was performed as above but using DAMMIF (11), and the best and worst χ^2 values were 1.17 and 1.23, respectively, with a model discrepancy of 0.73 ± 0.02. FOXS (12) was used for theoretical profile computation and data fitting. PyMOL (Schrodinger, LLC) and Chimera (13) were used for molecular rendering.

EM. G93A at ∼2 mg/mL was incubated in PBS containing 1 mM BME with 10 mM EDTA for 2.5 d and then diluted 1:100 in water. Three microliters were then placed on a copper–membrane–carbon grid that was plasma cleaned for 10 s using an argon/O_2 mixture. The sample was incubated for 60 s followed by a single slow blot with 2% uranyl formate that left a thin layer of the stain to air dry. Images were collected on a T2 (Tecnai F20 at 200 kV) microscope using a Tietz F416 CMOS camera using a dose of 45 $e^-/Å^2$.

Pulsed ESR Spectroscopy. SOD samples at ∼100–300 μM subunit concentrations were flash frozen in PBS containing 0.5 mM BME and 30% glycerol and maintained at 10 K during experiments. Observer pulses were made at 17.30 GHz, and the pump pulse was 17.15 GHz. After baseline correction, distances were reconstructed from the raw time domain data (e.g., as for WT in Fig. S7*A*) using the Tikhonov regularization (14) followed by the Maximum Entropy Method (15). Additional methodological details are described elsewhere (16).

1. Ahl IM, Lindberg MJ, Tibell LA (2004) Coexpression of yeast copper chaperone (yCCS) and CuZn-superoxide dismutases in Escherichia coli yields protein with high copper contents. *Protein Expr Purif* 37(2):311–319.
2. Lyons TJ, et al. (2000) The metal binding properties of the zinc site of yeast copper-zinc superoxide dismutase: Implications for amyotrophic lateral sclerosis. *J Biol Inorg Chem* 5(2):189–203.
3. de Beus MD, Chung J, Colón W (2004) Modification of cysteine 111 in Cu/Zn superoxide dismutase results in altered spectroscopic and biophysical properties. *Protein Sci* 13(5):1347–1355.
4. Goto JJ, Gralla EB, Valentine JS, Cabelli DE (1998) Reactions of hydrogen peroxide with familial amyotrophic lateral sclerosis mutant human copper-zinc superoxide dismutases studied by pulse radiolysis. *J Biol Chem* 273(46):30104–30109.
5. Stenlund P, Tibell LA (1999) Chimeras of human extracellular and intracellular superoxide dismutases. Analysis of structure and function of the individual domains. *Protein Eng* 12(4):319–325.
6. Classen S, et al. (2013) Implementation and performance of SIBYLS: A dual endstation small-angle X-ray scattering and macromolecular crystallography beamline at the Advanced Light Source. *J Appl Cryst* 46:1–13.
7. Konarev PV, Volkov VV, Sokolova AV, Koch MHJ, Svergun DI (2003) PRIMUS: A Windows PC-based system for small-angle scattering data analysis. *J Appl Cryst* 36:1277–1282.
8. Semenyuk AV, Svergun DI (1991) Gnom - a program package for small-angle scattering data-processing. *J Appl Cryst* 24:537–540.
9. Svergun DI (1999) Restoring low resolution structure of biological macromolecules from solution scattering using simulated annealing. *Biophys J* 76(6):2879–86.
10. Volkov VV, Svergun DI (2003) Uniqueness of ab initio shape determination in small-angle scattering. *J Appl Cryst* 36:860–864.
11. Franke D, Svergun DI (2009) DAMMIF, a program for rapid ab-initio shape determination in small-angle scattering. *J Appl Cryst* 42:342–346.
12. Schneidman-Duhovny D, Hammel M, Sali A (2010) FoXS: A web server for rapid computation and fitting of SAXS profiles. *Nucleic Acids Res* 38(web server issue): W540–W544.
13. Pettersen EF, et al. (2004) UCSF Chimera—a visualization system for exploratory research and analysis. *J Comput Chem* 25(13):1605–1612.
14. Chiang YW, Borbat PP, Freed JH (2005) The determination of pair distance distributions by pulsed ESR using Tikhonov regularization. *J Magn Reson* 172(2): 279–295.

15. Chiang YW, Borbat PP, Freed JH (2005) Maximum entropy: A complement to Tikhonov regularization for determination of pair distance distributions by pulsed ESR. *J Magn Reson* 177(2):184–196.

16. Merz GE, et al. (2014) Copper-based pulsed dipolar ESR spectroscopy as a probe of protein conformation linked to disease states. *Biophys J* 107(7):1669–1674.

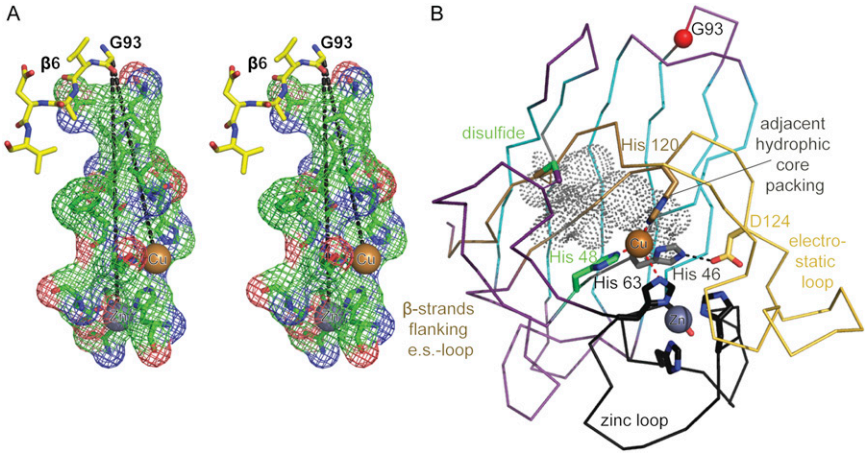

Fig. S1. Distances from key SOD structural elements to G93. (*A*) Stereo view image of G93 and the active site of one SOD subunit. The exposed G93 loop is connected to the active site metals (labeled spheres) through predictably stabilizing, dense-packing interactions (mesh) along ~19- and ~24-Å paths that transverse the β-barrel. This loop caps the β-barrel opposite the metals. (*B*) The copper site within Cu, Zn SOD is tied energetically into the β-barrel fold. All four copper histidine ligands are linked to key structural elements of the SOD framework. H46 resides adjacent to hydrophobic core residues F45, L117, and I18 (gray mesh). H48 resides near the disulfide formed between C57 and C146 (sea green). H63 forms part of the compact zinc loop (black). H120 links the electrostatic loop (yellow) to internal packing of the β-strands (two flanking strands shown in beige).

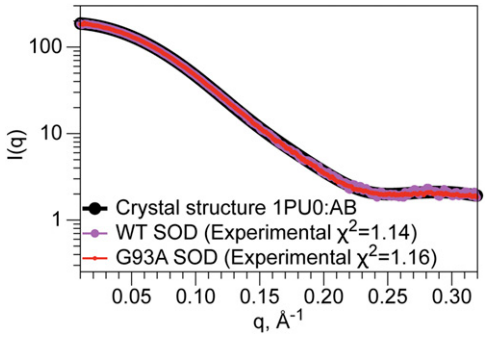

Fig. S2. SAXS profiles calculated for crystallographic WT SOD structure and measured experimentally for WT and G93A solution samples. SAXS intensity in detector units is plotted as a function of the scattering vector q ($q = 4\pi \sin\theta/\lambda$, where 2θ is the scattering angle), with the y axis plotted as log scale; the fit of the scattering data to the crystal structure (chains A and B) is indicated by χ^2 values.

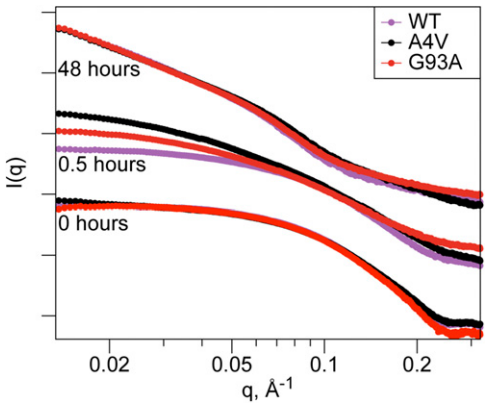

Fig. S3. Harsh treatment of WT and mutant SOD leads to production of similarly aggregated species. Combined EDTA and low pH conditions promote aggregation species for G93A, WT, and A4V control samples, although differences are noted at 0.5 h of treatment. Data are plotted as a power law (log–log) plot, with intensities (arbitrary units) from successive time points offset by 1 log for clarity.

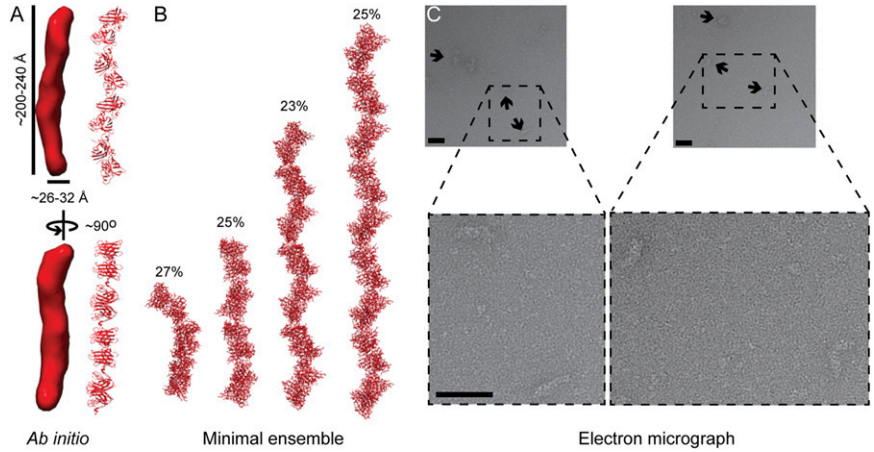

Fig. S4. Structural characterizations of metal-deficient G93A aggregates. (*A*) Ab initio modeling of 10 mM EDTA-treated G93A experimental SAXS data (1.25-d incubation with D_{max} estimate of 220 Å) suggests that signal-dominant SOD species are elongated, rod-like particles. However, these mass-averaged reconstruction models assume a homogeneous population. Assembly derived from the WT SOD structure [Protein Data Bank (PDB) ID code 1PU0] is shown next to the solid model for size-comparative purposes and fits the data with a χ^2 of 1.48. (*B*) Using a low *q* range of 0.0125–0.12, a minimal ensemble of elongated species is modeled for the same sample as in *A*. Fit of this species mixture with indicated percentages yields a χ^2 value of 0.74 (FOXS web server). Models are also based on extension of sets of dimers found within the WT SOD (PDB ID code 1PU0). (*C*) Transmission electron micrographs of 2.5-d incubated 10 mM EDTA-treated G93A aggregates stained with uranyl formate. Arrows indicate both clumpy/amorphous and elongated stained species of varying lengths. Dashed box regions are expanded below the full micrograph images. (Scale bar: 500 Å.)

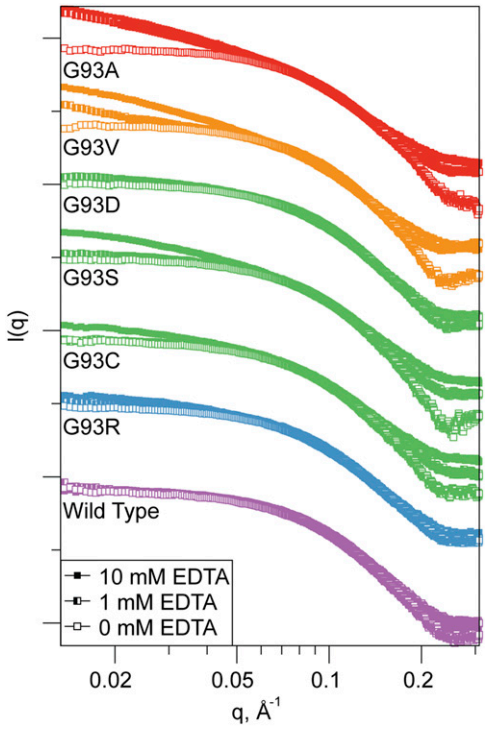

Fig. S5. Metal-chelated mutants containing free cysteines aggregate to varying extents based on EDTA concentration. WT SOD and G93 mutants treated for 30 h with 0 (empty squares), 1 (half-filled squares), or 10 mM (filled squares) were analyzed by SAXS. Data are plotted as a power law (log–log) plot, with intensities (arbitrary units) for each sample offset by 1 log for clarity.

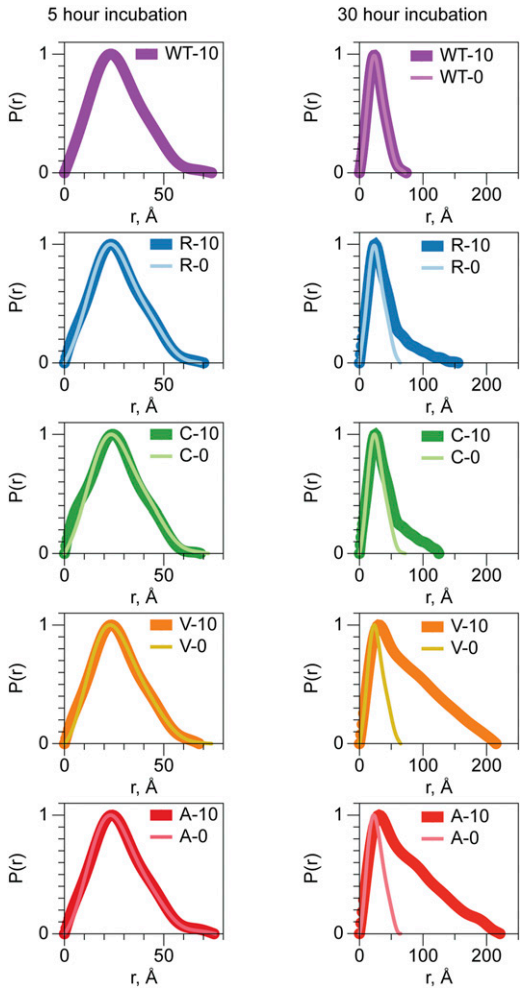

Fig. S6. Aggregation trajectory for WT and G93 mutant SODs. Real-space pairwise electron pair distributions, *P*(*r*), for selected G93 mutants representative of varying clinical severity and WT SOD reveal similarities of prenucleation species and larger aggregates. *P*(*r*) plots are normalized to peak height for ease of feature comparison. *Left* reveals data for samples incubated in 0 and 10 mM EDTA for 5 h. Note the subtle but consistent changes in *P*(*r*) features around 5, 15, and 35 Å. *Right* shows data for samples incubated in 0 and 10 mM EDTA for 30 h. Increasing propensity for aggregation of the mutants can be readily visualized by observing the D_{max} [where the *P*(*r*) curves intersect the abscissa] as a function of time in stress conditions. Note the similar changes in *P*(*r*) features around 45–50 Å with extended growth of all aggregates. Although data were not collected for the WT sample for the 0-mM EDTA 5-h incubation time point, WT SOD remained relatively unchanged after the 30-h incubation, irrespective of EDTA concentration. Similarly, *P*(*r*) plots for the WT samples incubated in 10 mM EDTA remained relatively unchanged between the two time points.

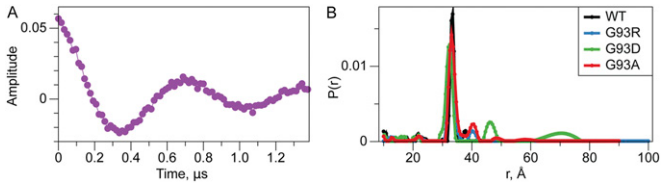

Fig. S7. Pulsed dipolar ESR spectroscopy data. (*A*) Representative raw time domain signal from WT SOD. (*B*) Full range of distance distribution data from Fig. 6*C*. Minor large-distance peaks are of unknown origin but may be artifacts of the distance reconstruction.

Table S1. Metal incorporation of recombinant SOD samples used in this work

Sample	Protein (μM)	Cu (μM)*	Zn (μM)*	Cu (%)	Zn (%)
Remetallated samples without CCS					
WT	6.4	5.3	11.2	82.6	175.7
WT-2[†]	222.0	132.0	258.1	59.5	116.2
G93A	9.4	3.2	10.9	33.9	116.4
G93A-2	6.1	1.7 (±0.1)	5.4 (±0.6)	26.7	82.8
G93C	9.1	4.1	6.7	44.5	73.2
G93D	4.3	1.4	5.3	32.7	122.2
G93R	11.4	5.8	14.4	50.6	126.4
G93S	11.1	3.7	9.4	33.7	84.9
G93V	7.2	2.8	8.1	39.2	112.3
Samples coexpressed with CCS					
WT	12.5	9.2 (±0.2)	9.3 (±0.5)	73.8	74.2
WT-2	12.5	9.3 (±1.0)	12.4 (±2.2)	74.2	99.1
WT-3	12.5	8.7 (±0.4)	12.8 (±1.3)	69.9	102.6
G93A	12.5	9.5 (±0.1)	9.1 (±0.3)	76.0	79.2
G93A-2	12.5	11.0 (±0.1)	13.8 (±0.7)	88.2	110.3
G93A-3	12.5	9.4 (±0.6)	13.1 (±1.3)	74.8	105.1
G93D	12.5	9.7 (±0.5)	6.2 (±0.4)	77.4	49.4
G93D-2	12.5	9.4 (±1.0)	13.3 (±1.6)	75.4	106.4
G93R	12.5	9.5 (±0.2)	10.0 (±0.2)	75.7	79.8
G93R-2	12.5	10.2 (±0.4)	8.8 (±0.6)	81.6	70.0
G93R-3	12.5	8.8 (±1.3)	12.3 (±1.7)	70.0	98.4
Samples treated for metal removal					
WT	12.5	2.5 (±0.1)	4.4 (±0.4)	20.3	35.1
G93A	12.5	1.6 (±0.2)	3.6 (±0.9)	12.5	28.7
G93D	12.5	1.9 (±0.1)	4.1 (±0.4)	14.9	32.4
G93R	12.5	2.0 (±0.2)	4.5 (±1.0)	16.2	35.8

Samples were analyzed by ICP-MS.

*Copper and zinc values are reported as the mean of two to three measurements of buffer-subtracted sample ± SD where applicable.

[†]No buffer was available for background correction of this sample.

Table S2. Sizes of SOD samples coexpressed with CCS and treated with 10 mM EDTA for 1 wk

1 wk + CCS	WT	G93R	G93A
R_g, Å	38.3	45.1	45.7
R_h, Å (% mass)*	41.7	47.4	49.9
R_c, Å	14.6	16.4	16.3

*DLS radius of hydration from major peak (≥99.4% by mass) determined by peak intensity.

Table S3. SAXS parameters derived from ALS mutants

Mutant	Expression	[EDTA], mM	Incubation, h	R_g, Å (Guinier)*	R_g, Å (real)	D_{max}, Å	R_c, Å†
WT	−CCS	0	0	20.8	20.9	66.5	N.D.
WT	−CCS	1	0	20.6	20.8	72.3	N.D.
WT	−CCS	10	0	20.5	20.7	72.9	N.D.
WT	−CCS	10	5	20.8	21.4	74.1	12.1
WT	−CCS	0	20	21.3	22	71.7	11.8
WT	−CCS	10	20	21.4	21.9	74.4	11.4
WT	−CCS	0	30	20.9	21.3	71.7	12.3
WT	−CCS	1	30	20.9	21.2	71.8	12.2
WT	−CCS	10	30	21.3	21.5	73.7	12
WT	+CCS	10	30	21.4	21.9	73.5	11.5
WT	+CCS	10	165	37.7	38.3	~126	13
G93A	−CCS	0	0	20.7	20.9	~70	N.D.
G93A	−CCS	1	0	20.7	20.9	70.9	N.D.
G93A	−CCS	10	0	20.6	20.8	70.9	N.D.
G93A	−CCS	0	5	20.5	21.6	76	12.5
G93A	−CCS	10	5	22	21.9	75.3	12.3
G93A	−CCS	0	20	22.7	22.2	76.6	12.3
G93A	−CCS	10	20	N.D.	27.8	~94	12.5
G93A	−CCS	0	30	21.3	20.8	67.1	12.1
G93A	−CCS	1	30	N.D.	61.3	~208	12.5
G93A	−CCS	10	30	N.D.	63.2	~221	12.8
G93A	+CCS	10	30	N.D.	25.7	~97	11.6
G93A	+CCS	10	165	N.D.	43.2	~140	16.2
G93A	+CCS	10	165	N.D.	45.7	~153	16.3
G93C	−CCS	0	5	21	21.4	72.4	12.4
G93C	−CCS	10	5	21	20.8	68.5	12.1
G93C	−CCS	0	30	21	21.3	71.6	12.3
G93C	−CCS	1	30	22.2	22.3	78.9	12.3
G93C	−CCS	10	30	N.D.	33.3	~125	12.1
G93D	−CCS	0	5	20.6	21	65.9	12.3
G93D	−CCS	10	5	20.8	21	67.6	12.4
G93D	−CCS	0	30	20.5	20.9	66.1	12.4
G93D	−CCS	1	30	N.D.	27.5	~115	12.4
G93R	−CCS	0	5	20.7	20.9	68.5	12.4
G93R	−CCS	10	5	20.7	21	70.2	12.1
G93R	−CCS	0	30	20.6	20.9	63.9	12.6
G93R	−CCS	1	30	22.6	24.3	~106	12.3
G93R	−CCS	10	30	N.D.	34.9	~155	12.3
G93R	+CCS	10	30	21.3	23	~85	12
G93R	+CCS	10	165	N.D.	45.5	~152	16.1
G93R	+CCS	10	165	N.D.	45.1	~146	16.4
G93S	−CCS	0	5	21.1	21.3	67	12.2
G93S	−CCS	10	5	20.7	21.1	70.6	12.2
G93S	−CCS	0	30	20.8	20.9	68.4	12.6
G93S	−CCS	1	30	N.D.	25.2	~99	12.3
G93S	−CCS	10	30	N.D.	49.5	~175	12.3
G93V	−CCS	0	5	20.7	21.2	74	12.5
G93V	−CCS	10	5	20.6	21.1	67.8	12.1
G93V	−CCS	0	30	21	21.1	64.7	12.3
G93V	−CCS	1	30	N.D.	58.4	~212	12.4
G93V	−CCS	10	30	N.D.	64.2	~215	13

N.D., not determined.

*$q \times R_g < 1.3$.

†$q \times R_c < 1.3$.